Longitudinal and transverse spin asymmetries for inclusive jet production at mid-rapidity in polarized $p + p$ collisions at $\sqrt{s} = 200$ GeV

L. Adamczyk,[1] G. Agakishiev,[20] M. M. Aggarwal,[31] Z. Ahammed,[50] A. V. Alakhverdyants,[20] I. Alekseev,[18] J. Alford,[21] B. D. Anderson,[21] C. D. Anson,[29] D. Arkhipkin,[3] E. Aschenauer,[3] G. S. Averichev,[20] J. Balewski,[25] A. Banerjee,[50] Z. Barnovska,[13] D. R. Beavis,[3] R. Bellwied,[46] M. J. Betancourt,[25] R. R. Betts,[9] A. Bhasin,[19] A. K. Bhati,[31] H. Bichsel,[52] J. Bielcik,[12] J. Bielcikova,[13] L. C. Bland,[3] I. G. Bordyuzhin,[18] W. Borowski,[43] J. Bouchet,[21] A. V. Brandin,[28] A. Bridgeman,[2] S. G. Brovko,[5] E. Bruna,[54] S. Bueltmann,[30] I. Bunzarov,[20] T. P. Burton,[3] J. Butterworth,[38] X. Z. Cai,[42] H. Caines,[54] M. Calderón de la Barca Sánchez,[5] D. Cebra,[5] R. Cendejas,[6] M. C. Cervantes,[44] P. Chaloupka,[13] S. Chattopadhyay,[50] H. F. Chen,[40] J. H. Chen,[42] J. Y. Chen,[8] L. Chen,[8] J. Cheng,[47] M. Cherney,[11] A. Chikanian,[54] W. Christie,[3] P. Chung,[13] J. Chwastowski,[10] M. J. M. Codrington,[44] R. Corliss,[25] J. G. Cramer,[52] H. J. Crawford,[4] X. Cui,[40] A. Davila Leyva,[45] L. C. De Silva,[46] R. R. Debbe,[3] T. G. Dedovich,[20] J. Deng,[41] R. Derradi de Souza,[7] S. Dhamija,[17] L. Didenko,[3] F. Ding,[5] A. Dion,[3] P. Djawotho,[44] X. Dong,[24] J. L. Drachenberg,[44] J. E. Draper,[5] C. M. Du,[23] L. E. Dunkelberger,[6] J. C. Dunlop,[3] L. G. Efimov,[20] M. Elnimr,[53] J. Engelage,[4] G. Eppley,[38] L. Eun,[24] O. Evdokimov,[9] R. Fatemi,[22] S. Fazio,[3] J. Fedorisin,[20] R. G. Fersch,[22] P. Filip,[20] E. Finch,[54] Y. Fisyak,[3] C. A. Gagliardi,[44] D. R. Gangadharan,[29] F. Geurts,[38] S. Gliske,[2] Y. N. Gorbunov,[11] O. G. Grebenyuk,[24] D. Grosnick,[49] S. Gupta,[19] W. Guryn,[3] B. Haag,[5] O. Hajkova,[12] A. Hamed,[44] L-X. Han,[42] J. W. Harris,[54] J. P. Hays-Wehle,[25] S. Heppelmann,[33] A. Hirsch,[35] G. W. Hoffmann,[45] D. J. Hofman,[9] S. Horvat,[54] B. Huang,[3] H. Z. Huang,[6] P. Huck,[8] T. J. Humanic,[29] L. Huo,[44] G. Igo,[6] W. W. Jacobs,[17] C. Jena,[15] J. Joseph,[21] E. G. Judd,[4] S. Kabana,[43] K. Kang,[47] J. Kapitan,[13] K. Kauder,[9] H. W. Ke,[8] D. Keane,[21] A. Kechechyan,[20] A. Kesich,[5] D. Kettler,[52] D. P. Kikola,[35] J. Kiryluk,[24] A. Kisiel,[51] V. Kizka,[20] S. R. Klein,[24] D. D. Koetke,[49] T. Kollegger,[14] J. Konzer,[35] I. Koralt,[30] L. Koroleva,[18] W. Korsch,[22] L. Kotchenda,[28] K. Kowalik,[24] P. Kravtsov,[28] K. Krueger,[2] L. Kumar,[21] M. A. C. Lamont,[3] J. M. Landgraf,[3] S. LaPointe,[53] J. Lauret,[3] A. Lebedev,[3] R. Lednicky,[20] J. H. Lee,[3] W. Leight,[25] M. J. LeVine,[3] C. Li,[40] L. Li,[45] W. Li,[42] X. Li,[35] X. Li,[41] Y. Li,[47] Z. M. Li,[8] L. M. Lima,[39] M. A. Lisa,[29] F. Liu,[8] T. Ljubicic,[3] W. J. Llope,[38] R. S. Longacre,[3] Y. Lu,[40] X. Luo,[8] A. Luszczak,[10] G. L. Ma,[42] Y. G. Ma,[42] D. M. M. D. Madagodagettige Don,[11] D. P. Mahapatra,[15] R. Majka,[54] O. I. Mall,[5] S. Margetis,[21] C. Markert,[45] H. Masui,[24] H. S. Matis,[24] D. McDonald,[38] T. S. McShane,[11] J. Millane,[24] S. Mioduszewski,[44] M. K. Mitrovski,[3] Y. Mohammed,[44] B. Mohanty,[50] M. M. Mondal,[44] B. Morozov,[18] M. G. Munhoz,[39] M. K. Mustafa,[35] M. Naglis,[24] B. K. Nandi,[16] Md. Nasim,[50] T. K. Nayak,[50] L. V. Nogach,[34] J. Novak,[27] G. Odyniec,[24] A. Ogawa,[3] K. Oh,[36] A. Ohlson,[54] V. Okorokov,[28] E. W. Oldag,[45] R. A. N. Oliveira,[39] D. Olson,[24] P. Ostrowski,[51] M. Pachr,[12] B. S. Page,[17] S. K. Pal,[50] Y. X. Pan,[6] Y. Pandit,[21] Y. Panebratsev,[20] T. Pawlak,[51] B. Pawlik,[32] H. Pei,[9] C. Perkins,[4] W. Peryt,[51] P. Pile,[3] M. Planinic,[55] J. Pluta,[51] D. Plyku,[30] N. Poljak,[55] J. Porter,[24] A. M. Poskanzer,[24] C. B. Powell,[24] D. Prindle,[52] C. Pruneau,[53] N. K. Pruthi,[31] M. Przybycien,[1] P. R. Pujahari,[16] J. Putschke,[53] H. Qiu,[24] R. Raniwala,[37] S. Raniwala,[37] R. L. Ray,[45] R. Redwine,[25] R. Reed,[5] C. K. Riley,[54] H. G. Ritter,[24] J. B. Roberts,[38] O. V. Rogachevskiy,[20] J. L. Romero,[5] J. F. Ross,[11] L. Ruan,[3] J. Rusnak,[13] N. R. Sahoo,[50] I. Sakrejda,[24] T. Sakuma,[44] S. Salur,[24] A. Sandacz,[51] J. Sandweiss,[54] E. Sangaline,[5] A. Sarkar,[16] M. Sarsour,[44] J. Schambach,[45] R. P. Scharenberg,[35] A. M. Schmah,[24] B. Schmidke,[3] N. Schmitz,[26] T. R. Schuster,[14] J. Seele,[25] J. Seger,[11] P. Seyboth,[26] N. Shah,[6] E. Shahaliev,[20] M. Shao,[40] B. Sharma,[31] M. Sharma,[53] S. S. Shi,[8] Q. Y. Shou,[42] E. P. Sichtermann,[24] R. N. Singaraju,[50] M. J. Skoby,[35] D. Smirnov,[3] N. Smirnov,[54] D. Solanki,[37] P. Sorensen,[3] U. G. deSouza,[39] H. M. Spinka,[2] B. Srivastava,[35] T. D. S. Stanislaus,[49] D. Staszak,[6] S. G. Steadman,[25] J. R. Stevens,[17] R. Stock,[14] M. Strikhanov,[28] B. Stringfellow,[35] A. A. P. Suaide,[39] M. C. Suarez,[9] M. Sumbera,[13] X. M. Sun,[24] Y. Sun,[40] Z. Sun,[23] B. Surrow,[25] D. N. Svirida,[18] T. J. M. Symons,[24] A. Szanto de Toledo,[39] J. Takahashi,[7] A. H. Tang,[3] Z. Tang,[40] L. H. Tarini,[53] T. Tarnowsky,[27] D. Thein,[45] J. H. Thomas,[24] J. Tian,[42] A. R. Timmins,[46] D. Tlusty,[13] M. Tokarev,[20] T. A. Trainor,[52] S. Trentalange,[6] R. E. Tribble,[44] P. Tribedy,[50] B. A. Trzeciak,[51] O. D. Tsai,[6] J. Turnau,[32] T. Ullrich,[3] D. G. Underwood,[2] G. Van Buren,[3] G. van Nieuwenhuizen,[25] J. A. Vanfossen, Jr.,[21] R. Varma,[16] G. M. S. Vasconcelos,[7] F. Videbæk,[3] Y. P. Viyogi,[50] S. Vokal,[20] S. A. Voloshin,[53] A. Vossen,[17] M. Wada,[45] F. Wang,[35] G. Wang,[6] H. Wang,[27] J. S. Wang,[23] Q. Wang,[35] X. L. Wang,[40] Y. Wang,[47] G. Webb,[22] J. C. Webb,[3] G. D. Westfall,[27] C. Whitten, Jr.,[6] H. Wieman,[24] S. W. Wissink,[17] R. Witt,[48] W. Witzke,[22] Y. F. Wu,[8] Z. Xiao,[47] W. Xie,[35] K. Xin,[38] H. Xu,[23] N. Xu,[24] Q. H. Xu,[41] W. Xu,[6] Y. Xu,[40] Z. Xu,[3] L. Xue,[42] Y. Yang,[23] Y. Yang,[8] P. Yepes,[38] Y. Yi,[35] K. Yip,[3] I-K. Yoo,[36] M. Zawisza,[51] H. Zbroszczyk,[51] J. B. Zhang,[8] S. Zhang,[42] W. M. Zhang,[21] X. P. Zhang,[47] Y. Zhang,[40] Z. P. Zhang,[40] F. Zhao,[6] J. Zhao,[42] C. Zhong,[42] X. Zhu,[47] Y. H. Zhu,[42] and Y. Zoulkarneeva[20]

(STAR Collaboration)

[1]*AGH University of Science and Technology, Cracow, Poland*
[2]*Argonne National Laboratory, Argonne, Illinois 60439, USA*
[3]*Brookhaven National Laboratory, Upton, New York 11973, USA*
[4]*University of California, Berkeley, California 94720, USA*
[5]*University of California, Davis, California 95616, USA*
[6]*University of California, Los Angeles, California 90095, USA*
[7]*Universidade Estadual de Campinas, Sao Paulo, Brazil*
[8]*Central China Normal University (HZNU), Wuhan 430079, China*
[9]*University of Illinois at Chicago, Chicago, Illinois 60607, USA*
[10]*Cracow University of Technology, Cracow, Poland*
[11]*Creighton University, Omaha, Nebraska 68178, USA*
[12]*Czech Technical University in Prague, FNSPE, Prague, 115 19, Czech Republic*
[13]*Nuclear Physics Institute AS CR, 250 68 Řež/Prague, Czech Republic*
[14]*University of Frankfurt, Frankfurt, Germany*
[15]*Institute of Physics, Bhubaneswar 751005, India*
[16]*Indian Institute of Technology, Mumbai, India*
[17]*Indiana University, Bloomington, Indiana 47408, USA*
[18]*Alikhanov Institute for Theoretical and Experimental Physics, Moscow, Russia*
[19]*University of Jammu, Jammu 180001, India*
[20]*Joint Institute for Nuclear Research, Dubna, 141 980, Russia*
[21]*Kent State University, Kent, Ohio 44242, USA*
[22]*University of Kentucky, Lexington, Kentucky, 40506-0055, USA*
[23]*Institute of Modern Physics, Lanzhou, China*
[24]*Lawrence Berkeley National Laboratory, Berkeley, California 94720, USA*
[25]*Massachusetts Institute of Technology, Cambridge, Massachusetts 02139-4307, USA*
[26]*Max-Planck-Institut für Physik, Munich, Germany*
[27]*Michigan State University, East Lansing, Michigan 48824, USA*
[28]*Moscow Engineering Physics Institute, Moscow, Russia*
[29]*Ohio State University, Columbus, Ohio 43210, USA*
[30]*Old Dominion University, Norfolk, Virginia, 23529, USA*
[31]*Panjab University, Chandigarh 160014, India*
[32]*Institute of Nuclear Physics PAS, Cracow, Poland*
[33]*Pennsylvania State University, University Park, Pennsylvania 16802, USA*
[34]*Institute of High Energy Physics, Protvino, Russia*
[35]*Purdue University, West Lafayette, Indiana 47907, USA*
[36]*Pusan National University, Pusan, Republic of Korea*
[37]*University of Rajasthan, Jaipur 302004, India*
[38]*Rice University, Houston, Texas 77251, USA*
[39]*Universidade de Sao Paulo, Sao Paulo, Brazil*
[40]*University of Science & Technology of China, Hefei 230026, China*
[41]*Shandong University, Jinan, Shandong 250100, China*
[42]*Shanghai Institute of Applied Physics, Shanghai 201800, China*
[43]*SUBATECH, Nantes, France*
[44]*Texas A&M University, College Station, Texas 77843, USA*
[45]*University of Texas, Austin, Texas 78712, USA*
[46]*University of Houston, Houston, Texas, 77204, USA*
[47]*Tsinghua University, Beijing 100084, China*
[48]*United States Naval Academy, Annapolis, Maryland 21402, USA*
[49]*Valparaiso University, Valparaiso, Indiana 46383, USA*
[50]*Variable Energy Cyclotron Centre, Kolkata 700064, India*
[51]*Warsaw University of Technology, Warsaw, Poland*
[52]*University of Washington, Seattle, Washington 98195, USA*
[53]*Wayne State University, Detroit, Michigan 48201, USA*
[54]*Yale University, New Haven, Connecticut 06520, USA*
[55]*University of Zagreb, Zagreb, HR-10002, Croatia*

We report STAR measurements of the longitudinal double-spin asymmetry A_{LL}, the transverse single-spin asymmetry A_N, and the transverse double-spin asymmetries A_Σ and A_{TT} for inclusive jet production at mid-rapidity in polarized $p + p$ collisions at a center-of-mass energy of $\sqrt{s} = 200$ GeV. The data represent integrated luminosities of 7.6 pb^{-1} with longitudinal polarization and 1.8 pb^{-1} with transverse

polarization, with 50%–55% beam polarization, and were recorded in 2005 and 2006. No evidence is found for the existence of statistically significant jet A_N, A_Σ, or A_{TT} at mid-rapidity. Recent model calculations indicate the A_N results may provide new limits on the gluon Sivers distribution in the proton. The asymmetry A_{LL} significantly improves the knowledge of gluon polarization in the nucleon.

I. INTRODUCTION

Deep-inelastic scattering (DIS) experiments with polarized lepton beams and targets containing polarized nucleons have measured the inclusive spin structure function $g_1(x, Q^2)$ of the nucleon over a wide range in Bjorken-x, $0.003 < x < 0.8$, and Q^2, $1 < Q^2 < 100$ GeV$^2/c^2$ [1–17]. The DIS data, combined with data on the couplings in neutron and hyperon β decay, lead one to conclude that the quark contribution to the spin of a longitudinally polarized nucleon is only about 25%, well below naive expectations that the nucleon spin originates mainly from the valence quarks. Perturbative QCD analyses [18–23] of the Q^2 dependence of $g_1(x, Q^2)$ gave the first insights into possible gluon polarization contributions, but the precision is thus far limited by the Q^2 range that is accessible in the fixed-target experiments. Semi-inclusive DIS spin asymmetry measurements with identified pions and kaons have made it possible to delineate the quark and antiquark spin contributions by flavor, and measurements with hadron pairs and open charm mesons have shown sensitivity to gluon polarization [24–28].

Collisions of polarized proton beams at the Relativistic Heavy Ion Collider (RHIC) at Brookhaven National Laboratory have made it possible to study proton spin structure via hadroproduction of jets and other hard probes at ten-fold higher center-of-mass energies than previous DIS experiments. Of particular interest to the determination of gluon polarization is the longitudinal double-spin asymmetry A_{LL},

$$A_{LL} = \frac{\sigma^{++} - \sigma^{+-}}{\sigma^{++} + \sigma^{+-}}, \quad (1)$$

where σ^{++} and σ^{+-} are the differential production cross sections when the beam protons have equal and opposite helicities, respectively. STAR has published differential production cross section data for inclusive jet production at mid-rapidity with transverse momenta, p_T, in the range $5 < p_T < 50$ GeV$/c$ [29] that are well described by perturbative QCD calculations at next-to-leading order (NLO) [30]. This supports the use of this framework in interpreting our measurements of A_{LL}.

Semi-inclusive deep-inelastic scattering experiments have also measured a broad range of transverse spin asymmetries (see for example [31–36]), including asymmetries sensitive to the Collins and Sivers effects. The Collins effect involves the convolution of quark transversity with the transverse-spin-dependent Collins fragmentation function, which has been measured in e^+e^- scattering [37,38]. The Sivers effect ascribes a spin-dependent transverse

momentum to the partons in a transversely polarized proton. Recently, global analyses have been performed to extract the quark transversity [39] and parton Sivers [40] distributions from the semi-inclusive DIS and e^+e^- data. Measurements of the transverse double-spin asymmetry, A_{TT}, for inclusive jet production provide a complementary probe of quark transversity [41]. It has also been proposed that the transverse single-spin asymmetry, A_N, for inclusive jet production may be sensitive to the Sivers effect [42].

In this article, we discuss the techniques that STAR uses to find and reconstruct inclusive jets in polarized $p + p$ collisions, update our earlier analysis of A_{LL} from 2005 data [43], and present precision data recorded in 2006 on A_{LL}. The A_{LL} results significantly improve our knowledge of the gluon polarization in the proton. We also present the first results for the transverse single-spin asymmetry A_N and transverse double-spin asymmetries A_Σ and A_{TT} (defined in Sec. IV B) for the inclusive production of mid-rapidity jets with transverse momenta up to 35 GeV$/c$ in polarized proton collisions at $\sqrt{s} = 200$ GeV. The A_N measurement may provide new limits on the gluon Sivers distribution in the proton [42].

II. EXPERIMENT AND DATA

A. RHIC-Star

A schematic diagram of the STAR detector at RHIC is shown in Fig. 1. The detector studies collisions of independently polarized proton beam bunches, ranging from 50–112 bunches stored in each of two rings for a given fill. During the 2005 run, the proton bunches were loaded with alternating spin directions for the beam that circulated in the clockwise direction (blue) and with alternating spins for successive pairs of bunches for the beam that circulated in the counterclockwise direction (yellow). More complex 8-bunch polarization patterns were implemented in 2006 to further reduce possible systematic errors associated with individual bunch patterns. Collisions at STAR are tagged by a coincidence of hits in the east and west beam-beam counters (BBC) [44], scintillation detectors that consist of 18 hexagonal tiles subtending the pseudorapidity interval, $3.4 < |\eta| < 5.0$, on opposite sides of the interaction region. The performance of this detector as a luminosity monitor was cross-checked against a pair of hadronic zero degree calorimeters (ZDCs) located ± 18 m from the detector center and at zero degrees relative to the beam axis.

STAR employs several subsystems for particle tracking and calorimetry [45]. The central time projection chamber
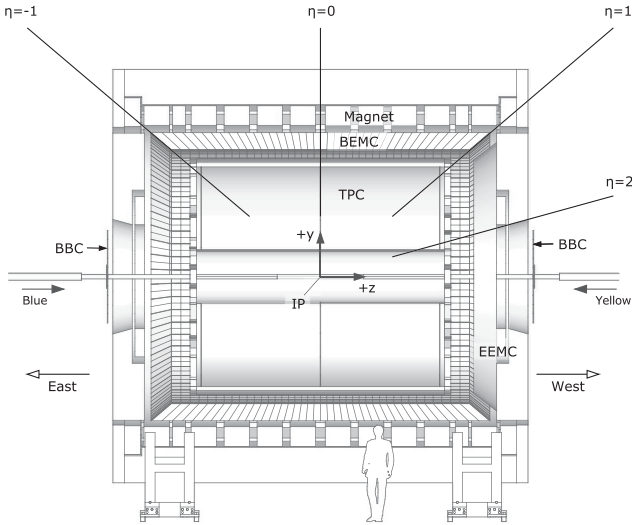
FIG. 1.   Schematic section cut of the STAR detector showing the detector elements used in these measurements.

(TPC) tracks charged particles with ∼85% efficiency over the full azimuth, $0 < \phi < 2\pi$, and pseudorapidity range, $|\eta| < 1.0$, and falling to ∼50% efficiency at $|\eta| \sim 1.3$. Surrounding the TPC is a barrel electromagnetic calorimeter (BEMC) that consists of 4800 Pb-scintillator towers covering the full azimuth over the range $-0.98 < \eta < +0.98$ in its final configuration. Each tower subtends an area of solid angle $(\Delta\phi \times \Delta\eta) = (0.05 \times 0.05)$. The positive η side of STAR (west end) is covered by an additional 720 Pb-scintillator towers comprising the endcap electromagnetic calorimeter, which extends calorimeter coverage over the full azimuth for the pseudorapidity range $1.08 < \eta < 2.0$. Both electromagnetic calorimeters are ∼20 radiations lengths and ∼1 strong interaction length deep. Fast signals from the calorimeter towers are processed to classify triggers for events of interest. The reader is referred to Ref. [45] for a comprehensive description of the STAR detector.

The measurements presented here were taken over two different running periods during the years 2005 and 2006. In 2005, only the west half of the BEMC ($0 < \eta < 0.98$) was available. Between the data-taking in 2005 and 2006, the BEMC commissioning was completed. This provided a more complete and robust picture of jets in our detector by doubling the acceptance and enabling measurements with jet cone radii, $R = \sqrt{\Delta\phi^2 + \Delta\eta^2} = 0.7$, which is larger than the value $R = 0.4$ that was used in our earlier analyses [29,43].

B. Triggers and data sets

A minimum-bias trigger was defined to be a coincidence between any pair of BBC tiles from opposite sides of the collision region. This trigger has been shown to accept about 87% of the nonsingly diffractive pp cross section [44]. A redundant set of scalers recorded BBC tile and plane hits for each RHIC beam crossing, allowing the

BBCs to be used as local luminosity monitors and polar-imeters. The scaler system also recorded numerous combinations of hit conditions, including hits in the BBC on opposite sides of the interaction region in 15 unequal intervals of the time difference between the hits. The intervals were chosen so as to give fine granularity for beam-beam collisions that occurred near the center of the detector ($z = 0$) and coarser granularity for events away from the center. We analyzed events from the intervals that correspond to a collision vertex selection along the beam direction of approximately ± 60 cm from the center of the detector. In this way, we matched the conditions for event selection with the conditions used in determining the relative luminosity for different spin combinations. The minimum-bias trigger was heavily prescaled to contribute only a few percent of the recorded data.

Triggers for the selection of events with jets were constructed by requiring substantial energy to be present in the BEMC. A high tower (HT) trigger was defined by requiring a BBC coincidence plus at least one BEMC tower with a transverse energy greater than a given threshold. A jet patch (JP) trigger required a BBC coincidence, plus a transverse electromagnetic energy in a region of $\Delta\eta \times \Delta\phi = 1.0 \times 1.0$ exceed a given threshold. The locations of the jet patches were fixed by hardware, with 12 such patches in the barrel calorimeter as shown in Fig. 2.

In 2005, data were taken with a mixture of HT and JP triggers with different thresholds. The low (high) HT1(2) triggers required each accepted event to have at least one BEMC tower with transverse energy $E_T > 2.6(3.5)$ GeV. The low (high) JP1(2) trigger thresholds were set to $E_T > 4.5(6.5)$ GeV. The HT1 and JP1 triggers were prescaled. There was considerable overlap among the triggers, with approximately half of the jets contained in the JP2 trigger sample.

In 2006, the JP trigger was operated with a threshold of $E_T > 7.8$ GeV early in the run, including the entire transverse polarization period. The threshold was then increased to 8.3 GeV for most of the longitudinal polarization period.
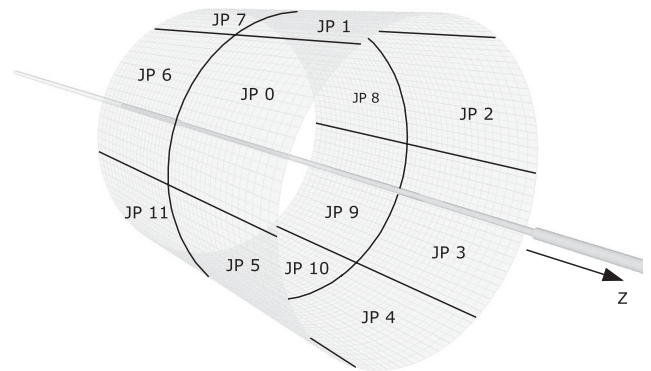

FIG. 2.   Schematic diagram showing the location of the fixed jet patches and calorimeter towers in the STAR barrel electromagnetic calorimeter.

Two additional triggers were also used. The first was a HT trigger that required $E_T > 5.4$ GeV. The second was a refinement of the HT trigger (HTTP) that required a high tower to exceed a threshold of 3.8 GeV, with an additional requirement of $E_T > 5.2$ GeV in the 3×3 array of towers centered on the high tower.

The integrated luminosity for longitudinally polarized beam was 2.1 pb^{-1} in 2005 and 5.5 pb^{-1} in 2006. The integrated luminosity for transversely polarized beam was 1.8 pb^{-1} during 2006.

III. JETS

Jets measure energy flow and are observable as composites of measured particle momenta. In the discussion below, we distinguish three categories: parton, particle, and detector jets. Our jet-finding and reconstruction method uses the approach and algorithm adopted from Ref. [46]. Parton jets are constructed from quarks and gluons either in theoretical calculations or in Monte Carlo simulated events prior to hadronization. Particle jets are constructed from the momenta of stable particles in Monte Carlo simulated events after hadronization. Detector jets are constructed from real or simulated data. An important difference compared to many other experiments is that the charged hadron momenta are measured in STAR with the TPC, rather than by a hadron calorimeter.

We use comparisons of parton-to-particle and particle-to-detector jets to quantify the corrections needed to account for contributions arising from spectator partons, effects of the underlying event in $p + p$ collisions, undetected energy from, for example, neutrons, K_L and neutrinos, particle scattering out of the jet cone due to the hadronization process, bias and resolution effects introduced by our triggers and detectors, and uncertainties in the relative contributions of different partonic processes that result from uncertainties in the parton distribution functions.

A. Jet-finding and reconstruction

Detector jets are reconstructed in this analysis using a midpoint cone algorithm [47] that combines charged tracks from the TPC and tower hits from the electromagnetic calorimeters. A primary vertex position is defined from the intersection of two or more charged tracks with the known transverse position of the beams. To be included in jet reconstruction, tracks are required to have a transverse momentum greater than 200 MeV/c, while tower hits must have a transverse energy E_T exceeding 200 MeV. Charged tracks are also required to contain $>20(>12)$ fit points in the TPC for 2005 (2006) and $>51\%$ of the maximum number of fit points allowed by the TPC geometry and active electronic channels. They are also required to have a distance-of-closest-approach to the primary vertex of dca < 3 cm. For the 2006 data, an additional p_T-dependent constraint was imposed on the transverse distance of the track from the beam line

(dcaD): dcaD < 2 cm for $p_T < 0.5$ GeV/c, dcaD < 1 cm for $p_T > 1$ GeV/c, and an interpolated cut in between. The tracking capabilities of the TPC generally allow a determination of the dca value with a resolution of 0.2–0.3 cm. These cuts are imposed to reduce pileup and background tracks in the data. Particles measured as TPC trajectories are assumed to be charged pions, whereas energy deposits in the electromagnetic calorimeters are assumed to be photons. To reduce double counting of energy, the average energy that a minimum-ionizing particle would deposit is subtracted from the calorimeter tower energy if a TPC track points to the tower. If the calculated minimum-ionizing particle energy deposition exceeds the energy observed in such a tower, the tower energy is discarded.

The midpoint cone algorithm begins by collecting a list of tracks and tower hits with transverse momentum/energy greater than a set threshold value. These tracks and towers serve as seeds for the initial jet cones or proto-jets, defined as the collection of track and tower four-momenta inside of a cone of radius R, whose axis coincides with the E_T-weighted centroid of the proto-jet four-momenta. Additional proto-jets are formed from the midpoints between seeds and added to the list. At this point, a single track or tower may contribute to several proto-jets.

Next, the algorithm decides whether to split or merge two proto-jets that have common four-momenta based on the fraction of energy shared by the two proto-jets. If the fraction is smaller than a specific value (0.5), the proto-jets are split into two jets and the shared four-momenta are assigned to the closest jets. If the fraction is greater than 0.5, the proto-jets are merged into a single jet. For 2005 data, the jet cone radius was chosen to be $R = 0.4$. The cone radius was increased to $R = 0.7$ for 2006 data to increase the efficiency and minimize the sensitivity to differences in the fragmentation of quark vs gluon jets. Parameters used in the jet-finding algorithm are summarized in Table I.

B. Event and jet cuts

Events were removed from this analysis in the absence of a valid polarization measurement, relative luminosity value or BBC vertex information, or if the event failed the offline verification of the trigger requirements. Events were also eliminated if the bunch identification tagged them as originating from noncolliding, diagnostic (or "kicked") bunches. Kicked bunches are special bunches whose betatron orbits are deliberately amplified in order to give a large amplitude signal to a beam position monitor. Timing measurements of the kicked bunches give more precise measurements of the energy of the beam. After these requirements, longitudinal data samples of 4.6M events were obtained in both 2005 and 2006.

Many of the events contain two or more reconstructed jets. For the spin asymmetry measurements, only those triggered jets that contain a trigger tower or point to a

TABLE I.   Midpoint cone algorithm parameters.

Parameter	2005 Jet finding	2006 Jet finding
Cone radius (rad)	0.4	0.7
Seed E_T threshold	0.5 GeV	0.5 GeV
Assoc. E_T threshold	0.1 GeV	0.1 GeV
Split/merge fraction	0.5	0.5
Track p_T threshold	0.2 GeV/c	0.2 GeV/c
Tower E_T threshold	0.2 GeV	0.2 GeV
Jet η	$0.2 < \eta < 0.8$	$-0.7 < \eta < 0.9$
Jet p_T	>5.0 GeV/c	>5.0 GeV/c

triggered jet patch are included. Events that contain both a triggered jet and a nontriggered jet were included in the sample used to estimate the beam gas background fraction (see next section). Further cuts, as described in the following sections, were imposed on the jets to eliminate backgrounds. After these requirements, the longitudinal data samples totaled 2.3 (2.1) M jets in 2005 (2006). Two percent (4%) of the events contained two jets, both of which passed all cuts.

C. Background events

1. Beam gas events

Energetic particles from beam gas scattering and other noncollision background sources can pass through the beam-line shielding and then shower in the electromagnetic calorimeters. Most of these events lack signals in at least one of the BBCs, so they fail the trigger requirement. Typically, they also fail our event cuts because they have no primary vertex within the active region of the TPC. However, such events can be mistaken for jets if they occur during beam crossings that also contain minimum-bias collisions.

It is extremely rare to have two energetic background particles enter STAR concurrently, so noncollision background events almost never contain two or more reconstructed jets. Also, background jets typically exhibit an abnormally large fraction of electromagnetic to total energy, referred to as the neutral energy fraction (NEF), due to the lack of charged particle tracks that point back to an allowed vertex. We use these features to identify the noncollision background contribution to our jet sample.

Figure 3 shows the neutral energy fraction distributions for our reconstructed jets when we divide them into two subsamples. The di-jet events contain a second reconstructed jet with $\Delta\phi > \pi/2$. To enhance the di-jet statistics, the second jet is not required to satisfy the trigger independently. It is also allowed to fall within a larger pseudorapidity range than normal because it is not essential to reconstruct its energy precisely. The monojet events are the remainder. The measured neutral energy distribution for di-jet events is well described by PYTHIA events processed through a GEANT model of the STAR detector (see Sec. III D). The monojet events are also well described
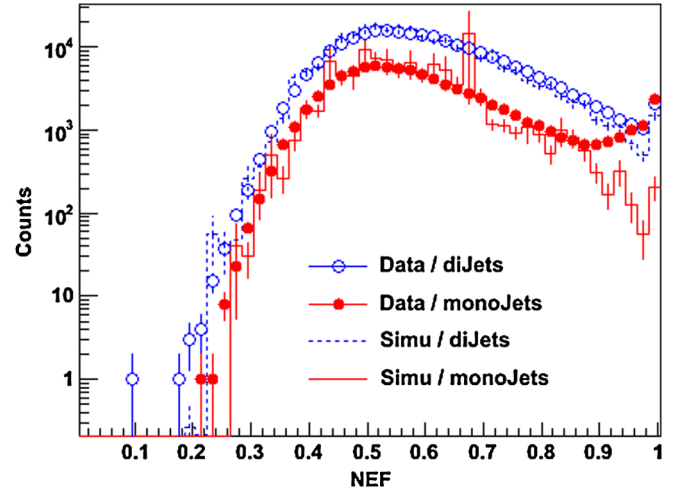
FIG. 3 (color online).   NEF distributions for mono- and di-jets for 2006 data (symbols) and Monte Carlo simulation (histograms). These events have uncorrected jet p_T in the range $14.08 < p_T < 17.31$ GeV/c.

except at large NEF, where a large enhancement due to noncollision background events is seen in the data.

The background component is determined from fits of the monojet to di-jet yield ratio as a function of NEF, as shown in Fig. 4. Signal events have a slowly varying ratio, which is well described by a linear dependence in Monte Carlo simulations. The charged energy that is reconstructed in noncollision background events arises from tracks that accidentally point toward the calorimeter energy deposition. These tracks are typically associated with the minimum-bias collision that was necessary to satisfy the trigger and produce a primary vertex. We find that this component can be fit with an exponential function.
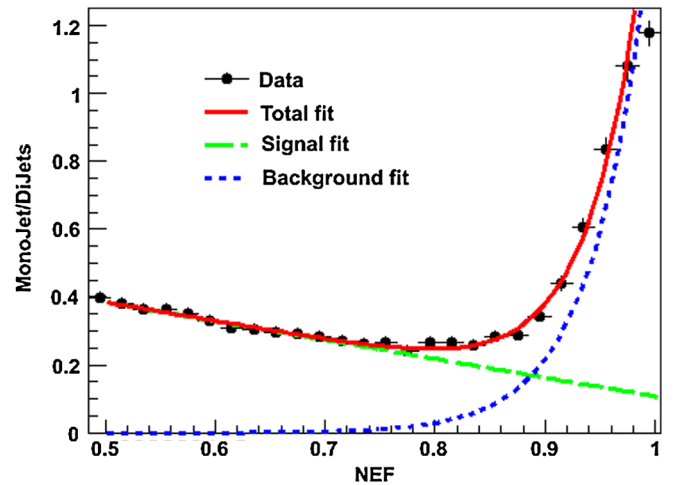
FIG. 4 (color online).   Fits of the mono/di-jet ratio vs NEF for 2006 data. The total fit (red solid curve) includes a decaying exponential for the background (blue dotted curve) and a first order polynomial for the signal (green dashed curve). These events have uncorrected jet p_T in the range $14.08 < p_T < 17.31$ GeV/c.

The background monojets with NEF > 0.95 were used to set an upper limit on the asymmetry in the noncollision backgrounds. We then established the cut for signal events to minimize the quadrature sum of the statistical and noncollision background uncertainties. For 2006, we required NEF < 0.92. Less shielding was present in 2005, so we required NEF < 0.90 for all bins except the lowest p_T bin. It was difficult to isolate the background component in the fit for the lowest 2005 p_T bin, leading to a very large uncertainty on any possible background asymmetry. Therefore, to be conservative we required NEF < 0.85 for this bin.

2. Electronlike events

Initial studies of the NEF distributions for the HT and HTTP triggered events found an enhancement in the jet yield for NEF in the range 0.4–0.5 in both the data and Monte Carlo simulations. The enhancement, which was particularly prevalent at low jet p_T, appeared primarily in the triggered monojet samples. The efficiency for observing the second jet in a di-jet increased with jet p_T, which indicated that the likely cause was events where the jet energy had been significantly overestimated. Further study determined that the enhancement arose from events where a conversion electron or positron that fired the HT or HTTP trigger also had a track reconstructed by the TPC. The jet finder will double-count the energy from such an electron or positron because it categorizes the TPC track and EMC tower as two high-energy particles with similar 4-vector E_T values.

A set of cuts was implemented to minimize the reconstruction bias associated with the double counting. Jets in HT or HTTP triggered events were discarded if the highest p_T track in the jet projected, within $|\Delta\eta| < 0.03$ and $|\Delta\phi| < 0.027$, to the location of the highest E_T tower. The ratio of the tower energy to track momentum was required to be less than 1.2. Figure 3 shows that these cuts effectively removed these "electronlike" events.

D. Simulations

Monte Carlo events were generated using PYTHIA 6.205 [48,49] (2005 data) and PYTHIA 6.410 [48,50] (2006 data) with parameters adjusted to the CDF "Tune A" settings [51] and processed through the STAR detector response package based on GEANT 3 [52], including simulation of the trigger electronics. The default PYTHIA parameter values, as well as those corresponding to this tune, are listed in Table II. In order to achieve a satisfactory simulation of the observed momentum balance for back-to-back jets (Fig. 5), we incorporated an intrinsic parton transverse momentum of 1 GeV/c into the default PYTHIA model. Small discrepancies with the data for these model calculations may still be observed; however, for the purpose of estimating the systematic uncertainties, the shapes of the data distributions are reproduced sufficiently well by the

TABLE II.   PYTHIA/CDF Tune A parameter values.

Parameter	PYTHIA 6.205	PYTHIA 6.410	CDF Tune A
MSTP(51)	7.0	7.0	7.0
MSTP(81)	1.0	1.0	1.0
MSTP(82)	1.0	4.1	4.0
PARP(82)	1.9	2.0	2.0
PARP(83)	0.5	0.5	0.5
PARP(84)	0.2	0.4	0.4
PARP(85)	0.33	0.9	0.9
PARP(86)	0.66	0.95	0.95
PARP(89)	1000	1800	1800
PARP(90)	0.16	0.16	0.25
PARP(91)	2.0	2.0	1.0
PARP(67)	1.0	4.0	4.0

simulations. We give further examples of the comparison of jet data and Monte Carlo in Figs. 6–8 for the jet p_T spectrum, track multiplicity, and integrated transverse energy profile within the jets. These figures use 2006 data and Monte Carlo simulations. They require each jet to satisfy at least one of the HT, JP, or HTTP trigger conditions, the same condition used in the asymmetry analysis. The effect of the triggers on the character of the jets is seen most readily in Fig. 9, which plots the NEF distribution of the jets for two different jet momentum ranges. At low momenta, the calorimeter-based triggers preferentially select jets with higher neutral energy fraction than jets at higher p_T. The systematic uncertainty associated with this
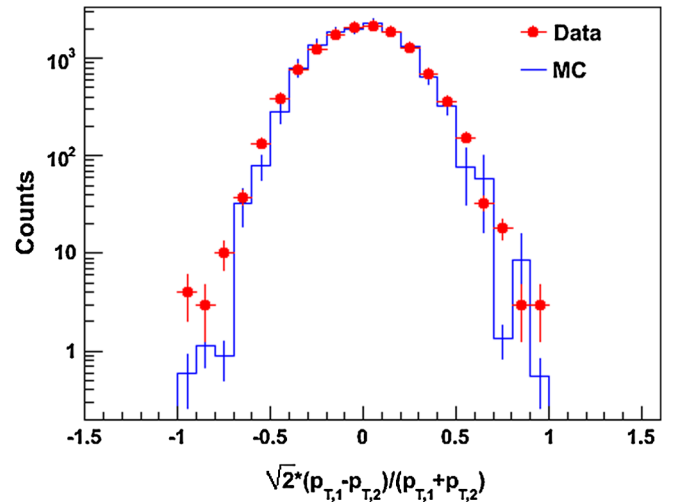
FIG. 5 (color online).   Relative difference in p_T for back-to-back di-jets for 2006 data. Both jets satisfy all cuts, including the trigger-matching requirement. These events have uncorrected jet p_T in the range $14.08 < (p_{T,1} + p_{T,2})/2 < 17.31$ GeV/c. For this case, we find ~5% discrepancy between data and Monte Carlo simulations. Essentially all the bins match simulations to within 10%. The p_T resolution is estimated to be ~23% from this graph.
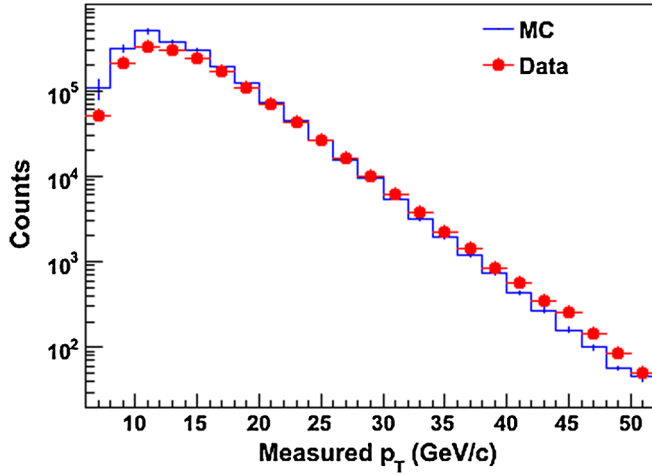
FIG. 6 (color online). Raw jet yield versus uncorrected jet transverse momentum in 2006 data (points) compared with Monte Carlo simulations (histogram).

FIG. 8 (color online). Fraction of the total jet transverse energy found within a cone of radius ΔR centered on the reconstructed thrust axis, illustrating the jet profile. Data from 2006 (symbols) and Monte Carlo simulations (curves) are shown for three different corrected jet p_T bins.
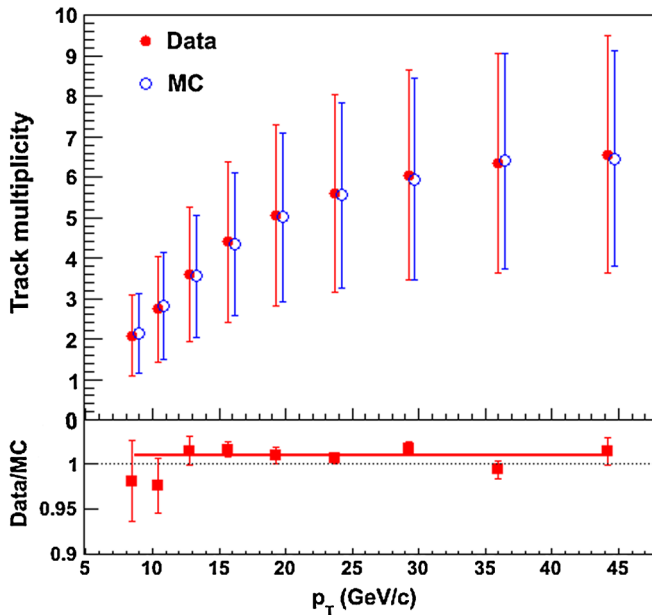

FIG. 7 (color online). Top: Average track multiplicity in the reconstructed jet vs jet p_T for 2006 data (solid symbols) and Monte Carlo simulations (open symbols). Vertical bars represent the rms width of the multiplicity distributions rather than the uncertainty on the mean. Bottom: Ratio of data to Monte Carlo simulations. Vertical bars show the statistical uncertainties.

FIG. 9 (color online). NEF for 2006 data (symbols) and Monte Carlo simulations (histograms) for uncorrected jet p_T in the ranges $7.6 < p_T < 9.3$ GeV/c (upper panel) and $39.6 < p_T < 48.7$ GeV/c (lower panel). These plots demonstrate the substantial bias introduced at low p_T by triggering on only electromagnetic energy.

trigger bias will be discussed below. Additional comparisons of underlying event properties between these STAR data and predictions from CDF Tune A may be found in Ref. [53].

E. Jet energy scale

Jet spin asymmetries are reported here as a function of the jet transverse momentum. However, a number of

corrections must be made to the physical measurements to permit comparisons to the parton-level cross sections and jet p_T definitions used in theoretical calculations. Some corrections are best subsumed into the systematic uncertainties on the asymmetries themselves, while others are more naturally applied as shifts to the jet momenta.

1. TPC and calorimeter calibration

The TPC calibration proceeds in several steps [54]. First, the drift velocity, which is monitored during runtime via laser ionization of the gas, is determined to an accuracy of approximately 0.03%. Then, distortion of the tracks due to misalignments of the readout sectors, drift distortions in the magnetic field, and construction imperfections are removed by examining extremely rigid tracks in different volumes of the TPC. Finally, the effects of space charge due to positive ion buildup at high event rates is monitored and corrected by examining the distance of closest approach to the presumed common vertex of an ensemble of tracks. This latter quantity is monitored as a function of instantaneous luminosity throughout the runs, and the corrections are updated periodically. The resulting hit errors on the tracks are in the range 300–550 μm. The overall momentum resolution of the TPC tracks is approximately $\Delta p_T/p_T \sim 0.01 + 0.005 p_T/(\text{GeV}/c)$ for $p_T < 10$ GeV$/c$ [55]. The TPC tracking efficiency is $\sim 85 \pm 5\%$.

The electromagnetic calorimeter was calibrated using a sample of identified electrons in the TPC data with momenta between 1.5 and 15 GeV$/c$ that satisfied strict geometrical and isolation conditions. The extrapolated trajectory was required to remain completely within a tower and the maximum energy of the nearest neighbors was limited. The tower calibration was then determined from the distribution of the ratio of energy observed in the towers divided by the momentum of the track. The variation of this ratio as a function of distance from the center of the tower was studied in data and Monte Carlo, and a correction was applied to compensate for this variation. The correction amounts to a maximum of 8% at the edge of the fiducial cut.

The total uncertainty in the calorimeter response to jets is estimated to be 4.8% for the present analysis. This includes the uncertainty from the electron calibration plus contributions from the uncertainty in the differential response of the calorimeter to hadronic vs electromagnetic energy and the ability of the Monte Carlo simulation to describe the precise light output from the scintillators when energy is deposited very close to the edge between two towers. The nominal full scale gain for the individual calorimeter towers was changed from 28 GeV in 2005 to 60 GeV in 2006. Therefore, the calorimeter gain uncertainties are independent between the two years, even though the fractional uncertainties are equal.

2. Jet p_T scale corrections

Our largest p_T correction accounts for the difference in particle and detector jet p_T scales. The combination of a steeply falling p_T dependence in the jet yield, and a jet transverse momentum resolution of $\sim 23\%$ (seen in Fig. 5) causes substantial bin migration. Thus, on average, lower momentum jets are reconstructed as higher momentum jets. The most straightforward method of dealing with this effect is to apply a p_T shift to correct the average value of the detector jet p_T within a bin.

This correction is calculated by comparing the p_T centroid for Monte Carlo simulations of particle versus detector jets, bin-by-bin and for each trigger type, that are then combined to produce the p_T shift for the data. The main systematic uncertainties on this p_T shift are due to assumptions about the proportions of different partonic subprocesses contributing to the jet spectrum. The uncertainties were estimated by recalculating the p_T shifts for different subprocesses in PYTHIA, taking the maximum deviation for any of them, then adding the statistical uncertainty in quadrature with this value. The smaller cone size used in 2005, compared to 2006, results in a larger asymmetry in the associated systematic error. Table III (2005) and Table IV (2006) give these corrections for both years. For each transverse momentum bin (first column) we give the mean detector jet p_T (second column) and the corrected mean particle jet p_T (third column). The fourth

TABLE III. Jet transverse momentum bins and corrections for 2005 data. For each p_T bin, the average detector jet p_T and the corrected particle jet p_T values are listed. Also shown are the evaluated uncertainties on these p_T values arising from the p_T-shift procedure, from the residual uncertainties in our detector simulations, and from the uncertainties on our hadronization and underlying event estimation and the unknown QCD scale. The sum in quadrature of these uncertainties is tabulated in the final column. All uncertainties are in units of GeV$/c$.

Measured p_T range (GeV$/c$)	$\langle p_T \rangle$ (GeV$/c$)	Corrected $\langle p_T \rangle$(GeV$/c$)	p_T shift uncertainty	Detector sim. uncertainty	Hadr/UE/QCD scale uncertainty	Total uncertainty
5.00–6.15	5.58	5.32	$+0.18/-0.24$	± 0.23	$+0.27/-0.15$	$+0.40/-0.36$
6.15–7.56	6.86	6.30	$+0.11/-0.09$	± 0.25	$+0.37/-0.28$	$+0.46/-0.39$
7.56–9.30	8.43	7.06	$+0.36/-0.04$	± 0.27	$+0.43/-0.34$	$+0.62/-0.44$
9.30–11.44	10.37	8.67	$+0.20/-0.16$	± 0.35	$+0.52/-0.39$	$+0.66/-0.55$
11.44–14.08	12.76	10.73	$+0.09/-0.07$	± 0.41	$+0.68/-0.54$	$+0.80/-0.68$
14.08–17.31	15.70	13.08	$+0.08/-0.07$	± 0.52	$+0.75/-0.54$	$+0.92/-0.75$
17.31–21.30	19.31	16.00	$+0.19/-0.22$	± 0.63	$+0.80/-0.50$	$+1.04/-0.83$
21.30–26.19	23.75	19.39	$+0.30/-0.33$	± 0.77	$+0.94/-0.53$	$+1.25/-0.99$
26.19–32.22	29.21	23.57	$+0.38/-0.29$	± 0.94	$+1.12/-0.61$	$+1.51/-1.16$
32.22–39.63	35.92	28.07	$+0.58/-0.40$	± 1.12	$+1.29/-0.65$	$+1.80/-1.36$

TABLE IV. Jet transverse momentum bins and corrections for 2006 data. Details are the same as given in the caption for Table III.

Measured p_T range (GeV/c)	$\langle p_T \rangle$ (GeV/c)	Corrected $\langle p_T \rangle$(GeV/c)	p_T shift uncertainty	Detector sim. uncertainty	Hadr/UE/QCD scale uncertainty	Total uncertainty
7.56–9.30	8.43	8.51	+0.52/ − 0.37	±0.35	±0.51	+0.81/ − 0.72
9.30–11.44	10.37	10.32	+0.30/ − 0.35	±0.40	±0.57	+0.76/ − 0.78
11.44–14.08	12.76	12.17	+0.25/ − 0.23	±0.46	±0.76	+0.92/ − 0.92
14.08–17.31	15.70	14.41	+0.08/ − 0.08	±0.55	±0.81	+0.98/ − 0.98
17.31–21.30	19.31	17.15	+0.21/ − 0.17	±0.66	±0.86	+1.10/ − 1.10
21.30–26.19	23.75	20.45	+0.13/ − 0.16	±0.80	±0.98	+1.27/ − 1.28
26.19–32.22	29.21	24.42	+0.10/ − 0.12	±0.97	±1.17	+1.52/ − 1.52
32.22–39.63	35.92	29.41	+0.22/ − 0.27	±1.17	±1.37	+1.82/ − 1.82
39.63–48.74	44.19	34.72	+0.90/ − 1.22	±1.38	±2.03	+2.61/ − 2.74

column in each table gives the estimated uncertainties on the p_T shift. The fifth column arises from uncertainties in jet energy scale due to possible inaccuracies in the calibration and performance of the TPC and EMC detectors. The comparison of particle and detector jets was repeated for a variety of calibration ranges, tracking inefficiencies, and detector states in order to estimate conservatively the range of possible effects on the p_T shift due to detector performance.

3. Pileup corrections

Pileup refers to the rate-dependent correction for charged tracks and calorimeter hits that were accidentally added to a jet during reconstruction. The largest pileup contribution came from out-of-time tracks that were nonetheless reconstructed within the 40 μs TPC readout period. Additional sources included multiple events within the same bunch crossing or beam halo background that was coincident with a hard collision.

To estimate the size of this correction, during normal data-taking a small fraction of events was taken with a random trigger, that is, data taken during nominal beam crossings, but with no detector requirements. These events are expected to contain the effects of the pileup energy alone, including the correct averaging over the instantaneous luminosity during the data-taking.

Jets were reconstructed in a sample of normal events. The tracks and calorimeter hits from random events in the same run were then added to these same normal events and a new set of jets were reconstructed. Separate average shifts were calculated for tracks and calorimeter hits and these average shifts were applied to the final jet p_T spectra. For 2005 (2006) this amounted to a shift of 0.008 (0.050) GeV/c per jet. The larger correction for 2006 reflects the larger cone size used in the jet reconstruction and the higher instantaneous luminosity that was available.

4. Hadronization and underlying event corrections

The p_T shift applied above is still not complete. There is a further difference in scale between parton jet momentum and particle jet momentum that may be divided into two partially compensating effects: underlying event (UE) and out-of-cone (OOC) [56] fragmentation.

The OOC effect causes a reduction of the measured p_T in particle jets due to fragmentation and hadronization of the parent parton outside of the jet cone. This correction may be subprocess dependent as quarks are expected to have a harder fragmentation spectrum than gluons. The underlying event causes an increase in the measured p_T in particle jets due to the inclusion of particles arising from interactions between spectator partons in the proton remnants and from additional hard partonic scatterings in the event. The UE is expected to be isotropic in $\eta \times \phi$ space and has been found to be largely independent of jet p_T.

The combined effect from the OOC and UE on the jet p_T scale was estimated by comparing reconstructed jets at the fragmented parton (FP) and particle (PART) level in events generated by the PYTHIA 6.3 Monte Carlo package [48,57] with parameters set to the CDF Tune A values. Jets at the FP stage contain only the fragmented partons resulting from the scattered partons and the initial and final radiation [MSTP(61), MSTP(71)]. At the FP stage the underlying event and hadronization [MSTP(81), MSTP(111)] are turned off. Note that MSTP(81) only controls the multiple parton interaction component of the UE and does not include effects from remnant interactions. Jets at the PART level contain the stable, hadronized, final-state particles resulting from the interaction in addition to any initial and final-state radiation. The reconstructed jet p_T scale at the PART level in simulations is comparable to the experimentally measured jet scale after corrections for detector resolution and trigger bias are included.

The total change in jet p_T scale, $\Delta p_T = p_T^{FP} - p_T^{PART}$, depends on the radius of the jet cone. Generally the shift is smaller for jets reconstructed with the larger cone radius in 2006. The reduced shifts at larger p_T for $R = 0.7$ indicates that OOC effects become less important as the cone radius increases. The lower p_T behavior is dominated by UE effects. As expected, the Δp_T was found to be subprocess dependent and larger for gluon jets. Therefore these effects have been included as a systematic uncertainty, instead of a correction, on

the measured detector + trigger corrected jet p_T. These uncertainties are given in the sixth columns of Tables III and IV.

IV. SPIN ASYMMETRY ANALYSIS

A. The spin asymmetry A_{LL}

Experimentally, the double longitudinal spin asymmetry defined in Eq. (1) was evaluated according to

$$A_{LL} = \frac{\sum (P_1 P_2)(N^{++} - rN^{+-})}{\sum (P_1 P_2)^2 (N^{++} + rN^{+-})}, \quad (2)$$

where $P_{1,2}$ denote the measured beam polarizations, N^{++} and N^{+-} denote the inclusive jet yields for equal and opposite proton beam helicity configurations, respectively, and r is the ratio of measured luminosities for the two helicity configurations. Each sum is performed over runs that last from 10 to 30 min so that the measurements are sampled on time scales faster than typical variations in the beam polarizations and relative luminosities.

1. Beam polarization

The beams are injected and circulated as bunches in the RHIC rings with their spins oriented in the vertical direction. Their polarizations are measured using Coulomb-nuclear interference polarimeters [58,59] that are calibrated against a polarized gas jet target [60] located at other interaction regions around the RHIC ring. The magnitude of the polarization is measured and monitored throughout the beam stores from these locations and is generally in the range from 50%–55%, with a statistical uncertainty of ~1%.

2. Relative luminosity

The relative luminosity for each polarization combination in a run was calculated from the sum of BBC coincidences over a run, after sorting bunches for each spin combination. Since these rates enter directly into the expression for the asymmetries, care was taken to ensure these data were consistent and systematically understood to a level commensurate with the size of the asymmetry being measured.

The BBC and ZDC analog pulses are discriminated and the coincidence signals are used as input signals to a time-to-amplitude converter, whose output is converted to a 4-bit time difference signal. For each beam crossing (every 106.5 ns), 4 bits for the BBC coincidence signal, 4 bits for the ZDC coincidence, and 7 bits for the beam crossing number are distributed to a set of 4 redundant scaler boards. These scaler data are then examined for statistical consistency; in general we find excellent agreement among all methods of luminosity measurement. However, a small fraction of runs ($< 1\%$) were rejected due to inconsistencies among the BBC measurements from different electronics channels.

As a further safeguard against detector failure or subtle physical effects, the BBC relative luminosity measurements were cross-checked against the ZDC measurements.

The BBCs are sensitive to the total nonsingly diffractive pp cross section by intercepting single charged particles over a broad rapidity range at moderate transverse momenta [44]. This hypothesis has been supported by PYTHIA calculations used in the design of these detectors, and by direct measurements (Vernier scans), which demonstrate that a very large fraction of the nonsingly diffractive cross section is indeed measured [61]. The ZDCs detect neutral particles like neutrons and π^0 s close to the rapidity of the beam, and are thus sensitive to types of collisions that are very different from those sampled by the BBCs. The small acceptance of the ZDCs limits the statistical precision of this comparison (for the present data); however, this has the additional advantage of allowing an examination of rate dependence of the luminosity measurements as well. The result of this comparison was consistent between the two years and gives a conservative systematic uncertainty on the relative luminosity of slightly less than 10^{-3}.

Corrections to the luminosity are expected due to accidental coincidences and undercounting of multiple interactions in a single beam crossing, as explained in Ref. [62]. These effects have been examined for the *relative* luminosities encountered in the 2005/2006 runs and found to be negligible compared to the systematic uncertainty assigned to the relative luminosity by comparing BBC and ZDC measurements.

B. Transverse spin asymmetries

In the 2006 run, STAR recorded 1.8 pb^{-1} of jet data from transversely polarized proton-proton collisions. These data have been analyzed in order to measure the transverse spin asymmetries A_N, A_Σ, and A_{TT}.

In a coordinate system where the positive z axis and pseudorapidity are defined by the momentum direction of beam 1, the polarization directions of the beams are along the y axis, and the azimuthal angle ϕ is defined relative to the x axis, we can write the jet production cross section for the two transversely polarized protons as in Ref. [63]:

$$d\sigma_{\text{pol}}/d\sigma_{\text{unpol}}$$
$$= 1 + P_1 P_2 \cdot A_\Sigma(\eta, p_T) + \cos(\phi) \cdot [P_1 \cdot A_N(\eta, p_T)$$
$$- P_2 \cdot A_N(-\eta, p_T)] + P_1 P_2 \cdot \cos(2\phi) \cdot A_{TT}(\eta, p_T).$$
$$(3)$$

Additional transverse spin asymmetries can be defined related to particle correlations within a jet [42,64] that are beyond the scope of this paper.

The extraction of the asymmetries proceeded as follows. The single-spin asymmetry, A_N, was determined by combining the spin directions for one beam to approximate an unpolarized "target." The single-spin asymmetry for each beam was determined separately, using the cross-ratio technique [65], and the results combined. The statistical precision for this measurement was sufficient to allow measurements as a function of jet transverse momentum

in 4 bins of pseudorapidity relative to the polarized beam, as shown in Fig. 10.

The double-spin asymmetry A_Σ was determined by averaging over the entire range of pseudorapidity and azimuth, using analysis procedures identical to those for A_{LL}. The results for A_Σ are given in Fig. 11. We are not aware of any theoretical predictions for A_Σ. However, it plays an important role in the estimation of the systematic uncertainty in A_{LL} due to residual transverse spin components in the beam (see Sec. IV C 2). A statistically significant measurement of A_{TT} could be made only by averaging over the full data set and extracting the coefficient of the $\cos(2\phi)$ dependence on the azimuthal angle from the fit shown in Fig. 12. We find $A_{TT} = -0.0049 \pm 0.0046$. This precision is not yet

FIG. 11 (color online). A_Σ versus corrected mean p_T for 2006 transverse data, averaged over the range $|\eta| < 0.8$. A_Σ, the transverse double-spin asymmetry for transversely polarized beams, is defined in more detail in the text.
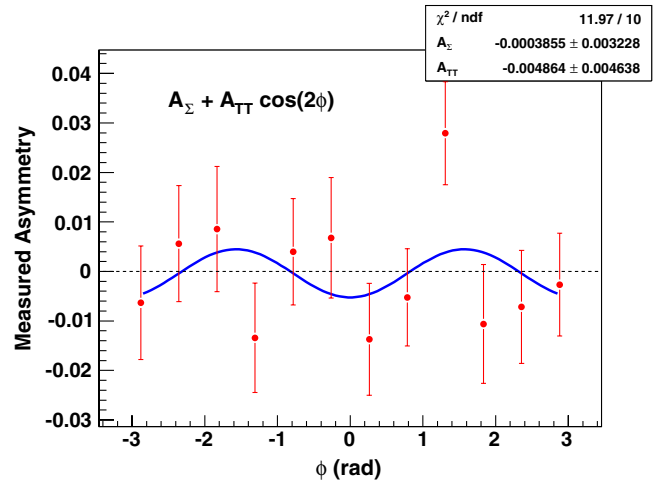
FIG. 12 (color online). Measured transverse double-spin asymmetry versus azimuthal angle ϕ for 2006 transverse data. The points are fit with the function $A_\Sigma + A_{TT} \cos(2\phi)$. These data are averaged over $7.5 < p_T < 40$ GeV/c and $|\eta| < 0.8$.

sufficient to confront predictions of A_{TT} due to quark transversity [41].

C. Systematic uncertainties

1. Trigger and reconstruction bias

Jet p_T resolution effects shown in Fig. 5 cause averaged shifts in the jet p_T scale as discussed in the previous section. Additionally, jet events are selected based on neutral energy triggers, that preferentially select jets with characteristics that differ from those of the unbiased jet distribution. For example, for the same jet momentum, the HT trigger will preferentially fire on jets with a high-energy leading particle while the JP trigger will fire on jets with larger radii. The relative
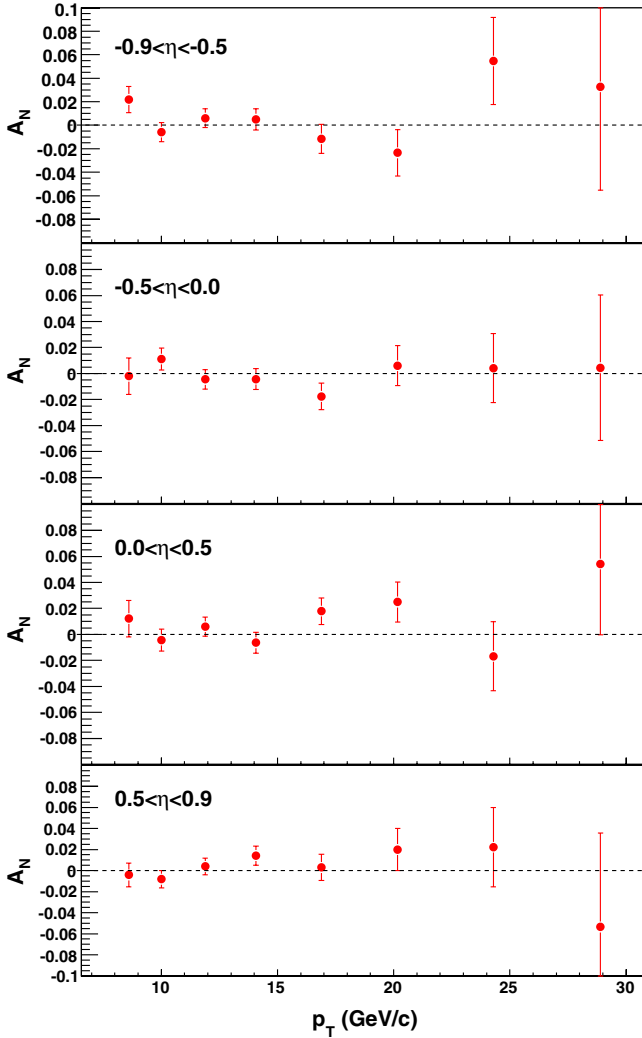

FIG. 10 (color online). A_N as a function of the corrected mean p_T for 2006 transverse data. The panels present A_N for four different η bins. A_N is the left-right single-spin asymmetry for a transversely polarized beam. The errors shown combine the statistical uncertainties, which dominate, with all systematic uncertainties except trigger and reconstruction bias. See Sec. V A for a discussion of the latter.
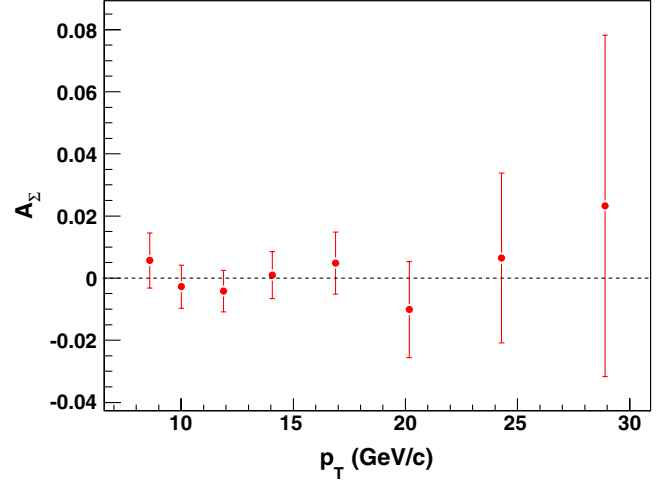
proportions of quark-quark, quark-gluon, and gluon-gluon interactions in an unbiased sample of events are fixed predominantly by the (well-determined) unpolarized structure functions. However, effects of the trigger and jet reconstruction can change the relative proportions in our measured sample, and this can bias our measurements of A_{LL} and A_N.

Calculation of the biases introduced by our trigger and jet reconstruction further depends on assumptions of the polarized parton structure functions. Our calculations must account for the uncertainty in polarized gluon contributions and, to a lesser degree, the associated uncertainties in polarized quark and sea contributions.

Parameterizations of the polarized parton distribution functions are combined with PYTHIA parton kinematic variables to generate predictions of A_{LL} vs p_T specific to a particular model at both the particle and detector levels. A broad range of polarized parton distribution functions were adopted for these calculations. Eventually, only those that predict distributions for A_{LL} vs p_T consistent with the general trends of our measured results were included in the bias estimate.

The method of calculating the trigger and reconstruction bias is then as follows. Relative fractions of jets resulting from HT, JP, and HTTP triggered events have been measured in data and found to agree with simulations. The logical OR of the three trigger types is therefore used to measure the trigger bias. For each p_T bin and polarized parton distribution model, A_{LL} is calculated both at the particle and detector levels. Detector A_{LL} points are shifted as discussed above to correct to the particle jet p_T scale. The residual difference between the particle jet A_{LL} and the shifted detector jet A_{LL} represents the bias for that model and p_T bin. To be conservative, the systematic uncertainty for each bin is assigned to be the largest positive and negative difference of all the allowed models. In Fig. 13 we show the result of this calculation for five representative models. The GRSV $+0.3$ and GRSV -0.3 models [66,67]
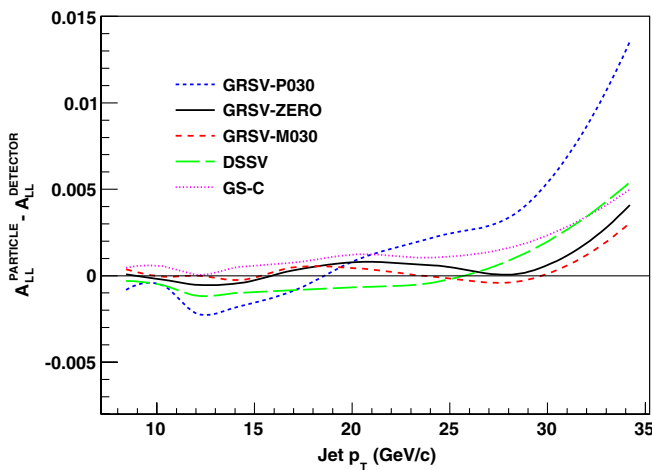

FIG. 13 (color online). Trigger and reconstruction bias estimates for the longitudinal double-spin asymmetry A_{LL} versus jet p_T for a representative set of polarized parton distribution models [20,66–68].

use the GRSV functional form for the gluon polarization, with the integral fixed at the two respective values. DSSV [68] is a recent fit that includes input data from RHIC, in addition to DIS and semi-inclusive DIS. GS-C [20] is an early model that has a large gluon polarization at low x. These five models span a range in gluon polarization that is wider than permitted by our results. The systematic uncertainties as a function of p_T are listed in the second column of Tables V and VI.

2. False asymmetries from residual transverse spin effects

False asymmetries that mimic our A_{LL} signal can arise from a combination of physical and experimental sources. To obtain longitudinal collisions at STAR, the transversely polarized beams are rotated to the longitudinal direction, then back again to transverse on either side of the interaction region by a pair of helical dipoles known as spin rotators. Inaccuracies in the adjustment of the spin rotator currents leave small transverse components for both beams in the collision region. Our transverse spin asymmetry measurements allow us to put stringent limits on the associated false asymmetries.

The transverse asymmetries in the central rapidity region are expected (and measured) to be small. However, in the presence of nonlongitudinal polarization components, the asymmetry A_Σ can contribute directly to the observed A_{LL} signal. Local measurements of the transverse polarization components of both beams during *longitudinal* running were made by examining the single-spin asymmetries observed in BBC tile hits. The transverse single-spin asymmetry (A_N) has been reported previously for this detector [44,69]. As given in these references, it is in the range of $\sim$6–7 $\times 10^{-3}$ and can be calibrated to a high accuracy during *transverse* running. Because the BBC is a highly segmented detector, combinations of up/down and left/right scatterings can be used to measure the transverse polarization components for both beams. These measurements were made continuously through the data-taking. The residual transverse components for both beams during the nominally longitudinal run were weighted by integrated luminosity for different periods of adjustment for the spin rotators. Denoting the angle of the polarization with the longitudinal axis as θ, values of $\tan(\theta)$ between 0.02–0.18 were measured, with an average magnitude equal to $\sim$0.1 for both beams.

Because measurements of A_Σ were consistent with zero, we do not make a correction to A_{LL} for this contribution, but instead assign a systematic uncertainty on our A_{LL} measurements. We combined the measurements of the transverse polarization components with the *uncertainties* on the measurements of A_Σ in each momentum bin to give a conservative (maximal) estimate of the systematic uncertainty:

$$\delta A_{LL} = |\tan(\theta_1)\tan(\theta_2)\cos(\phi_1 - \phi_2) \times A_\Sigma|$$
$$\sim |\theta_1 \theta_2 \delta A_\Sigma|, \tag{4}$$

TABLE V. p_T-dependent systematic uncertainties for 2005 data. The trigger and jet reconstruction bias, nonlongitudinal beam polarization, and beam gas background systematic uncertainties on the measured 2005 A_{LL} are given.

p_T (GeV/c)	Trigger bias and jet recon. ($\times 10^{-3}$)	Nonlongitudinal pol. ($\times 10^{-4}$)	Beam gas background ($\times 10^{-4}$)
5.32	$-1.67/+1.67$	± 4.97	± 13.50
6.30	$-1.47/+1.29$	± 2.49	± 8.07
7.06	$-1.44/+1.10$	± 1.54	± 7.97
8.67	$-1.80/+2.66$	± 1.20	± 8.40
10.73	$-1.24/+2.32$	± 1.16	± 6.82
13.08	$-1.34/+2.50$	± 1.31	± 5.34
16.00	$-1.88/+2.86$	± 1.74	± 4.55
19.39	$-2.74/+2.74$	± 2.69	± 3.51
23.57	$-3.91/+3.91$	± 4.75	± 0.50
28.07	$-3.44/+5.60$	± 9.56	± 0.00

TABLE VI. p_T-dependent systematic uncertainties for 2006 data. Details are the same as given in the caption for Table V.

p_T (GeV/c)	Trigger bias and jet recon. ($\times 10^{-3}$)	Nonlongitudinal pol. ($\times 10^{-4}$)	Beam gas background ($\times 10^{-4}$)
8.51	$-2.00/+3.37$	± 0.90	± 15.17
10.32	$-1.07/+1.97$	± 0.71	± 7.66
12.17	$-1.26/+1.99$	± 0.68	± 4.92
14.41	$-0.58/+1.11$	± 0.77	± 3.43
17.15	$-0.43/+0.70$	± 1.02	± 3.57
20.45	$-0.72/+1.52$	± 1.58	± 4.48
24.42	$-1.03/+3.92$	± 2.79	± 7.52
29.41	$-1.57/+5.46$	± 5.61	± 7.92
34.72	$-2.88/+6.93$	± 12.85	± 5.01

where $\theta_1(\theta_2)$ and $\phi_1(\phi_2)$ are the polar and azimuthal angles of the polarization vectors for beams 1 (2), respectively. In keeping with the spirit of estimating this uncertainty conservatively, the value of $\cos(\phi_1 - \phi_2)$ was set equal to unity. The uncertainty on A_{LL} due to nonlongitudinal components of the beams as a function of p_T is listed in the third column of Tables V and VI.

3. Beam gas background

The systematic uncertainty on the residual beam background was conservatively estimated to be the larger of either the measured effect or the statistical uncertainty of the measured effect on the asymmetry. These numerical values range from $\sim 15 \times 10^{-4}$ in the smallest p_T bins to less than half this value at higher p_T. This uncertainty as a function of p_T is listed in the fourth column of Tables V and VI.

4. Polarization and relative luminosity

Systematic errors arising from beam polarization and relative luminosity measurements are treated separately due to their correlated effects on the data. An error in the relative luminosity measurement would result in a shift of the A_{LL} data points by an additive constant, while an error

in the measurement of the polarization magnitude would scale the magnitude of the A_{LL} data. Therefore we quote these quantities separately.

The systematic uncertainty on the relative luminosity was determined by comparing the BBC and ZDC measurements, which were found to be consistent at the $<10^{-3}$ level. The BBC-ZDC difference was used to estimate the possible size of the uncertainty on A_{LL} due to the errors on the relative luminosity as $\delta A_{LL} \sim 9 \times 10^{-4}$ for both 2005 and 2006 data.

The fractional systematic uncertainty for the quantity $P_1 P_2$ quoted by the RHIC CNI polarimeter group (common to all RHIC experiments) is 9.4% (8.3%) for 2005 (2006) [70]. Polarization measurements from different years have contributions which may be identified as either uncorrelated or correlated. The total error was conservatively estimated by assuming the latter portion to be 100% correlated from year to year. The correlated error in the normalization of beam polarizations comes mostly from an unpolarized molecular hydrogen background in the gas jet polarization measurement. These errors represent an overall scale uncertainty on our measurements, and are common with the polarization uncertainties of concurrent measurements performed by the PHENIX experiment. They are therefore

quoted separately to facilitate comparison of different data sets and to identify correlated errors, where possible.

D. False asymmetries

All measurements were examined as a function of time to ensure the absence of nonstatistical variations. In addition, the data for different beam and bunch combinations were combined to form parity-violating single and double-spin asymmetries. These are expected to be highly suppressed and provide internally consistent cross-checks on the validity of the measurements. Double-spin asymmetries were formed from the "like-sign" and "unlike-sign" bunch combinations, and single-spin longitudinal asymmetries were formed for each beam direction. No false asymmetry was found to be significantly different from zero.

V. RESULTS AND DISCUSSION

A. A_N Results

In a recent model calculation, D'Alesio $et\ al.$ [42] conclude that A_N for inclusive jets at mid-rapidity arises solely from the gluon Sivers effect. Within their model, the leading contribution to the systematic uncertainty on our measured inclusive jet A_N arises from the fact that our triggers have different efficiencies for detecting jets from either quark-quark, quark-gluon, or gluon-gluon scattering. Although the latter two processes dominate at low jet p_T, the detector efficiency is largest for quark-quark scattering. This can lead to a measured A_N that is smaller in magnitude than the true value. We have used our Monte Carlo simulations to estimate the size of this effect. We find that correcting for this bias would increase the magnitude of A_N by up to 40% for low-p_T jets, dropping to 25% at 15 GeV/c and 15% at 30 GeV/c.

D'Alesio $et\ al.$ find that the current upper limit on the gluon Sivers distribution would lead to $|A_N|$ of 4%–5% at $p_T = 8$ GeV/c, dropping to $\sim$2.5% at 15 GeV/c [42]. The results in Fig. 10 indicate that our measured A_N is substantially smaller than these upper limits. Thus, they may provide new constraints on the magnitude of the gluon Sivers distribution in the proton.

B. A_{LL} results

The different detector geometries, triggers, jet definitions, and measured pseudorapidity ranges of the two different data-taking years reported here have demanded independent evaluations of the asymmetries and systematic uncertainties. While the list of corrections from both years are the same, individual items differ in magnitude and range from year to year. Furthermore, the different jet definitions and pseudorapidity intervals for the two years lead to different expectations for A_{LL} from model calculations. We therefore do not combine the results from different years, but present them separately. Our results from year 2005 data are given in Fig. 14 and Table VII. The
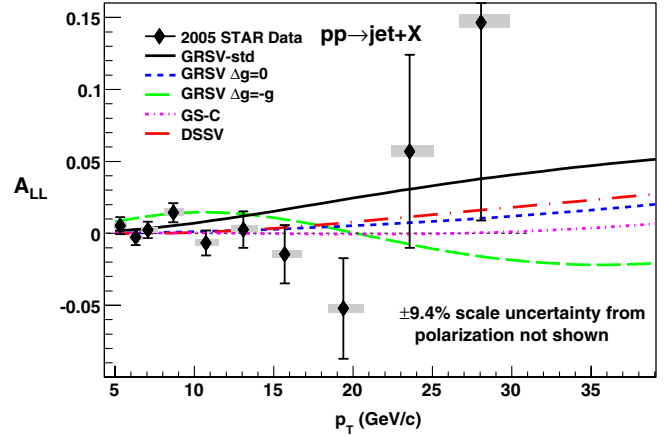

FIG. 14 (color online). A_{LL} for inclusive jet production versus corrected jet p_T for 2005 data. For 2005 data we used a cone radius equal to 0.4 and a pseudorapidity range for the jet thrust axis of $0.2 < \eta < 0.8$. The error bars are statistical. The gray boxes show the systematic uncertainties.

corresponding results for year 2006 data are given in Fig. 15 and Table VIII. Note the different scales on the vertical axes for the two figures.

C. Comparison to theory

The theoretical curves shown in Figs. 14 and 15 are derived from NLO calculations of spin asymmetries based on the code of Jager $et\ al.$ [30]. This code provides both the polarized and unpolarized proton-proton cross sections for an input cone of radius R centered at rapidity y and averaged over azimuth to $O(3)$ in α_s. Expressions for all $2 \rightarrow 2$ and $2 \rightarrow 3$ processes were derived analytically in a

TABLE VII. The final measured A_{LL} and p_T values from the 2005 data sample. Data cover the range $0.2 < \eta < 0.8$ with a jet cone radius of $R = 0.4$. Statistical and systematic uncertainties are listed for A_{LL} (note the systematic uncertainty is asymmetric as described in the text). The p_T-dependent corrections listed in Table V were combined in quadrature with the systematic uncertainty of 9×10^{-4} in relative luminosity to give the total. The p_T values shown are the results after applying all p_T corrections discussed in the text.

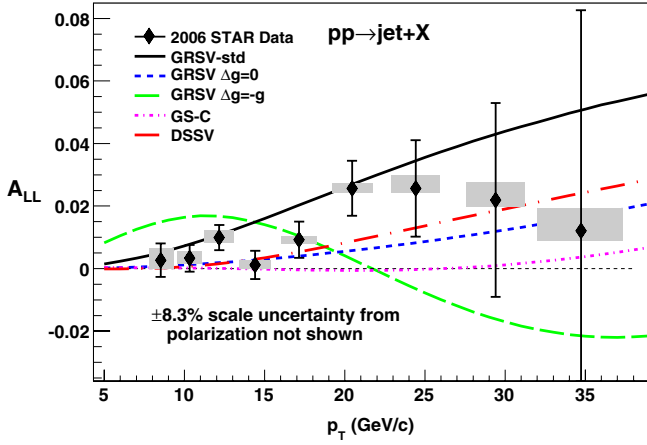| p_T (GeV/c)	A_{LL} ($\times 10^{-3}$)	Stat. err. ($\times 10^{-3}$)	Sys. err. ($\times 10^{-3}$)
$5.3 + 0.4/ - 0.4$	5.3	± 5.9	$+2.4/ - 2.4$
$6.3 + 0.5/ - 0.4$	-2.7	± 5.4	$+1.8/ - 1.9$
$7.1 + 0.6/ - 0.4$	2.4	± 5.7	$+1.7/ - 1.9$
$8.7 + 0.7/ - 0.6$	14.3	± 6.7	$+2.9/ - 2.2$
$10.7 + 0.8/ - 0.7$	-6.7	± 8.7	$+2.6/ - 1.7$
$13.1 + 0.9/ - 0.8$	2.6	± 12.7	$+2.7/ - 1.7$
$16.0 + 1.0/ - 0.8$	-14.6	± 20.3	$+3.0/ - 2.2$
$19.4 + 1.3/ - 1.0$	-52.2	± 35.0	$+2.9/ - 2.9$
$23.6 + 1.5/ - 1.2$	56.9	± 67.1	$+4.1/ - 4.1$
$28.1 + 1.8/ - 1.4$	146	± 138	$+5.7/ - 3.7$

FIG. 15 (color online). A_{LL} for inclusive jet production versus corrected jet p_T for 2006 data. For 2006 data we used a jet cone radius equal to 0.7 and a pseudorapidity range of $-0.7 < \eta < 0.9$ to reflect the increased detector coverage. The error bars are statistical. The gray boxes show the systematic uncertainties.

small cone approximation, with the subsequent integrals evaluated numerically using a Monte Carlo approximation. The results were compared to more complete calculations [71] also using Monte Carlo evaluation of the integral, but without the small cone assumption [30].

The code allows as input the colliding energy of the protons, the jet cone radius, the jet rapidity, and the jet transverse momentum intervals for integration of the cross section. The code requires assumptions for two scale inputs: the initial-state factorization scale (μ_I) and the renormalization scale (μ_R). We take the value $\mu_I = \mu_R = p_T$ of the jets. The polarized and unpolarized inclusive jet cross sections are calculated by separate programs.

As originally configured, the programs require polarized and unpolarized parton distribution functions that are sampled by the Monte Carlo portions of the program

TABLE VIII. The final measured A_{LL} and p_T values from the 2006 data sample. Data cover the range $-0.7 < \eta < 0.9$ with a jet cone radius of $R = 0.7$. Details are the same as given in the caption for Table VII.

p_T (GeV/c)	A_{LL} ($\times 10^{-3}$)	Stat. err. ($\times 10^{-3}$)	Sys. err. ($\times 10^{-3}$)
$8.5 + 0.8/ -0.7$	2.7	± 5.3	$+3.8/ -2.6$
10.3 ± 0.8	3.3	± 4.3	$+2.3/ -1.6$
12.2 ± 0.9	9.9	± 4.1	$+2.3/ -1.6$
14.4 ± 1.0	1.2	± 4.5	$+1.5/ -1.2$
17.2 ± 1.1	9.2	± 5.8	$+1.2/ -1.1$
20.5 ± 1.3	25.7	± 8.8	$+1.8/ -1.3$
24.4 ± 1.5	25.6	± 15.4	$+4.1/ -1.6$
29.4 ± 1.8	22.0	± 31.0	$+5.6/ -2.1$
$34.7 + 2.6/ -2.7$	12.0	± 70.6	$+7.1/ -3.3$

over a wide range of x and Q^2. These are tabulated at fixed values beforehand and interpolated to the required precision. The original configuration also allowed for a selection among several sets of unpolarized (CTEQ5, CTEQ6M, CTEQ6M.1) and polarized (GRSV2000 STND, MAX, MIN, ZERO) parton distribution functions. All calculations here use the pdf set CTEQ6M [72] and a cone radius of 0.4 or 0.7, as noted.

The possible size of higher order corrections to the cross sections is conventionally estimated by varying the factorization and renormalization scales by a factor of 2 about the nominal scale. In Fig. 16, we plot calculations that show the scale dependence of the relative asymmetry, A_{LL}/A_{LL}^0, as a function of jet transverse momentum for both jet cone radii. In this expression, A_{LL}^0 is the asymmetry calculated with the nominal scales $\mu_{I,R} = p_T$, while A_{LL} is calculated for scales of $2p_T$ and $p_T/2$. The parton distribution functions used in this calculation were the CTEQ6 set and GRSV2000 STND. In general, the larger the cone radius, the less sensitive is the calculation of the spin asymmetry (not cross section) with respect to scale and higher order contributions. The choice of cone radius equal to 0.4 for 2005 was made in consideration of the size of the (instrumented) part of the detector, in order that acceptance uncertainties would not dominate the systematic uncertainty on the jet energy. With increased EMC coverage in year 2006, our sensitivity to scale variations is lessened.

The impact of these data on previous constraints of the integral of the polarized gluon distribution function, ΔG, from deep-inelastic lepton scattering data is shown in Figs. 14 and 15 and is quantified in a recent global analysis
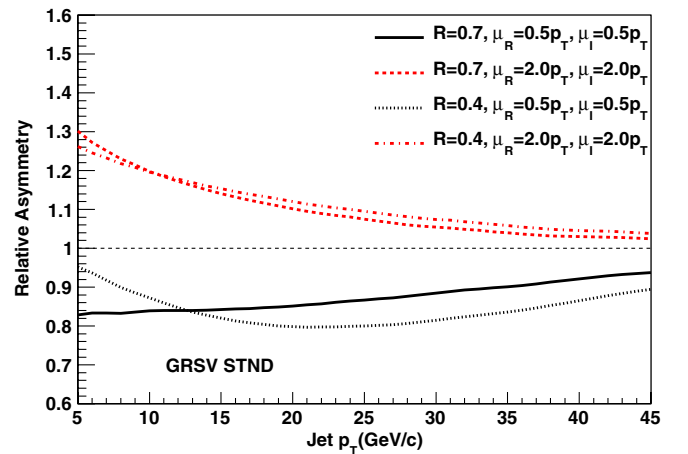

FIG. 16 (color online). Scale dependence of the relative asymmetry (defined in the text) as a function of jet transverse momentum. The asymmetry is calculated for the GRSV standard set of parameters. The black (red) lines are the ratios of the asymmetries calculated for half (twice) the nominal renormalization and initial-state scales of $\mu_R = \mu_I = p_T$. The dotted curves are for a jet cone radius of 0.4 and solid and dashed curves are for a cone radius of 0.7.

[68] that includes the preliminary data values from this analysis. The measured A_{LL} values are seen to lie in the region below the previous best-fit DIS curve, GRSV standard [30,66,67]. The remaining curves associated with GRSV are the polarized parton distributions refit to constrain ΔG to a series of values spanning the full range $-g(x) \leq \Delta g(x, Q_0^2) \leq g(x)$, that is the gluon spins may be fully polarized in either direction, or interpolated to intermediate values using a common functional form.

Data from a single experiment cover a limited kinematic range in x and Q^2, making the measurement of the total integral $\Delta G(Q^2)$ at a specific Q^2 impossible. A rigorous extraction of ΔG requires the incorporation of these inclusive jet asymmetries, along with other RHIC, DIS, and SIDIS polarized scattering data, into a global analysis. For example, the AAC analysis [73] demonstrated that while the inclusion of PHENIX pion longitudinal double-spin asymmetries [74] available at that time had only a small influence on the optimum fit, the uncertainties on the gluon polarized parton distribution function were significantly reduced over the fit obtained using DIS data alone.

This type of analysis, more recently performed by de Florian *et al.* (DSSV) [23,68], uses NLO pQCD fits to the world data set (including the STAR 2005 [43] and a preliminary version of the 2006 jet asymmetries presented here), constrained by a functional form that defines $\Delta g(x, Q^2)$ in the unmeasured regions of x space, to extract the spin-dependent parton densities. The DSSV global analysis is based on Mellin moments, which allows a certain amount of x integrated data to be included in the fits. This is an especially important development for RHIC data, where the statistical precision within our kinematical constraints thus far only allows the examination of ΔG over a limited range of $0.05 < x < 0.2$. The DSSV best fit finds the gluon polarization to be much smaller than that in GRSV standard throughout the x region, which is currently constrained by data. Furthermore, in the x region sampled by RHIC data the DSSV $\chi^2 + 2\%$ upper limit on $\Delta g(x, Q^2)$ at $Q^2 = 10$ GeV^2 is roughly half the GRSV standard value (see Fig. 2 in [68]).

VI. SUMMARY

In summary, we have reported an analysis of spin dependencies in the inclusive production of mid-rapidity jets with transverse momenta up to 35 GeV/c in polarized $p + p$ collisions at $\sqrt{s} = 200$ GeV from data recorded in 2005 and 2006. No evidence is found for the existence of statistically significant transverse asymmetries A_N, A_Σ, and A_{TT}. The A_N result may provide new limits on the gluon Sivers distribution in the proton. The longitudinal double-spin asymmetry A_{LL} has been compared with NLO perturbative QCD evaluations based on selected polarized parton distribution functions to demonstrate its sensitivity to the value of the gluon helicity distribution inside the proton.

[1] J. Ashman *et al.*, Phys. Lett. B **206**, 364 (1988).
[2] J. Ashman *et al.*, Nucl. Phys. **B328**, 1 (1989).
[3] P. L. Anthony *et al.* (E142 Collaboration), Phys. Rev. D **54**, 6620 (1996).
[4] K. Ackerstaff *et al.*, Phys. Lett. B **404**, 383 (1997).
[5] K. Abe *et al.*, Phys. Lett. B **405**, 180 (1997).
[6] K. Abe *et al.*, Phys. Rev. Lett. **79**, 26 (1997).
[7] B. Adeva *et al.*, Phys. Rev. D **58**, 112001 (1998).
[8] K. Abe *et al.*, Phys. Rev. D **58**, 112003 (1998).
[9] P. L. Anthony *et al.*, Phys. Lett. B **463**, 339 (1999).
[10] P. L. Anthony *et al.*, Phys. Lett. B **493**, 19 (2000).
[11] X. Zheng *et al.*, Phys. Rev. C **70**, 065207 (2004).
[12] X. Zheng *et al.*, Phys. Rev. Lett. **92**, 012004 (2004).
[13] A. Airapetian *et al.*, Phys. Rev. D **71**, 012003 (2005).

[14] K. V. Dharmawardane *et al.*, Phys. Lett. B **641**, 11 (2006).
[15] V. Y. Alexakhin *et al.*, Phys. Lett. B **647**, 8 (2007).
[16] A. Airapetian *et al.*, Phys. Rev. D **75**, 012007 (2007).
[17] M. G. Alekseev *et al.*, Phys. Lett. B **690**, 466 (2010).
[18] J. Blümlein and H. Böttcher, Nucl. Phys. **B841**, 205 (2010).
[19] E. Leader, A. V. Sidorov, and D. B. Stamenov, Phys. Rev. D **82**, 114018 (2010).
[20] T. Gehrmann and W. J. Stirling, Phys. Rev. D **53**, 6100 (1996).
[21] R. D. Ball, S. Forte, and G. Ridolfi, Phys. Lett. B **378**, 255 (1996).
[22] D. de Florian, G. A. Navarro, and R. Sassot, Phys. Rev. D **71**, 094018 (2005).

[23] D. de Florian, R. Sassot, M. Stratmann, and W. Vogelsang, Phys. Rev. D **80**, 034030 (2009).
[24] M. Alekseev *et al.*, Phys. Lett. B **676**, 31 (2009).
[25] A. Airapetian *et al.*, Phys. Rev. Lett. **84**, 2584 (2000).
[26] B. Adeva *et al.*, Phys. Rev. D **70**, 012002 (2004).
[27] E. S. Ageev *et al.*, Phys. Lett. B **633**, 25 (2006).
[28] A. Airapetian *et al.*, J. High Energy Phys. 08 (2010) 130.
[29] B. I. Abelev *et al.*, Phys. Rev. Lett. **97**, 252001 (2006).
[30] B. Jäger, M. Stratmann, and W. Vogelsang, Phys. Rev. D **70**, 034010 (2004).
[31] A. Airapetian *et al.*, Phys. Rev. Lett. **94**, 012002 (2005).
[32] M. Alekseev *et al.*, Phys. Lett. B **673**, 127 (2009).
[33] A. Airapetian *et al.*, Phys. Rev. Lett. **103**, 152002 (2009).
[34] M. Alekseev *et al.*, Phys. Lett. B **692**, 240 (2010).
[35] A. Airapetian *et al.*, Phys. Lett. B **693**, 11 (2010).
[36] X. Qian *et al.*, Phys. Rev. Lett. **107**, 072003 (2011).
[37] R. Seidl *et al.*, Phys. Rev. Lett. **96**, 232002 (2006).
[38] R. Seidl *et al.*, Phys. Rev. D **78**, 032011 (2008).
[39] M. Anselmino, M. Boglione, U. D'Alesio, A. Kotzinian, F. Murgia, A. Prokudin, and S. Melis, Nucl. Phys. B, Proc. Suppl. **191**, 98 (2009).
[40] M. Anselmino, M. Boglione, U. D'Alesio, A. Kotzinian, S. Melis, F. Murgia, A. Prokudin, and C. Türk, Eur. Phys. J. A **39**, 89 (2009).
[41] J. Soffer, M. Stratmann, and W. Vogelsang, Phys. Rev. D **65**, 114024 (2002).
[42] U. D'Alesio, F. Murgia, and C. Pisano, Phys. Rev. D **83**, 034021 (2011).
[43] B. I. Abelev *et al.*, Phys. Rev. Lett. **100**, 232003 (2008).
[44] J. Adams *et al.*, Phys. Rev. Lett. **91**, 172302 (2003); L. C. Bland, arXiv:hep-ex/0403012; J. Kiryluk *et al.*, arXiv:hep-ex/0501072.
[45] K. H. Ackermann *et al.*, Nucl. Instrum. Methods Phys. Res., Sect. A **499**, 624 (2003), and references therein.
[46] T. Aaltonen *et al.*, Phys. Rev. D **78**, 052006 (2008); **79**, 119902(E) (2009).
[47] G. C. Blazey *et al.*, arXiv:hep-ex/0005012.
[48] T. Sjöstrand, P. Edén, C. Friberg, L. Lönnblad, G. Miu, S. Mrenna, and E. Norrbin, Comput. Phys. Commun. **135**, 238 (2001).
[49] T. Sjöstrand, L. Lönnblad, and S. Mrenna, arXiv:hep-ph/0108264.

[50] T. Sjöstrand, S. Mrenna, and P. Skands, J. High Energy Phys. 05 (2006) 026.
[51] R. Field and R. C. Group (CDF), arXiv:hep-ph/0510198.
[52] GEANT 3.21, CERN Program Library.
[53] H. Caines *et al.*, Nucl. Phys. **A830**, 263C (2009); H. Caines *et al.*, Nucl. Phys. **A855**, 376 (2011).
[54] G. Van Buren *et al.*, Nucl. Instrum. Methods Phys. Res., Sect. A **566**, 22 (2006).
[55] J. Adams *et al.*, Phys. Lett. B **637**, 161 (2006).
[56] A. Bhatti *et al.*, Nucl. Instrum. Methods Phys. Res., Sect. A **566**, 375 (2006).
[57] T. Sjöstrand, L. Lönnblad, S. Mrenna, and P. Z. Skands, arXiv:hep-ph/0308153.
[58] O. Jinnouchi *et al.*, arXiv:nucl-ex/0412053.
[59] H. Okada *et al.*, Phys. Lett. B **638**, 450 (2006).
[60] H. Okada *et al.*, arXiv:hep-ex/0601001.
[61] A. Drees *et al.*, BNL PAC Proceedings (2003).
[62] D. Cronin-Hennessy, A. Beretvas, and P. F. Derwent, Nucl. Instrum. Methods Phys. Res., Sect. A **443**, 37 (2000).
[63] F. Rathmann *et al.*, Phys. Rev. C **58**, 658 (1998).
[64] F. Yuan, Phys. Rev. Lett. **100**, 032003 (2008).
[65] G. G. Ohlsen and P. W. Keaton, Nucl. Instrum. Methods **109**, 41 (1973).
[66] M. Glück, E. Reya, M. Stratmann, and W. Vogelsang, Phys. Rev. D **63**, 094005 (2001).
[67] M. Stratmann and W. Vogelsang (private communication).
[68] D. de Florian, R. Sassot, M. Stratmann, and W. Vogelsang, Phys. Rev. Lett. **101**, 072001 (2008).
[69] J. Kiryluk, AIP Conf. Proc. **675**, 424 (2003).
[70] See http://www4.rcf.bnl.gov/~cnipol/pubdocs/NOTE_ 2005_2006_Comb_Pol.txt for posts by the RHIC polarimetry group of official results for the polarization vs fill for any given year.
[71] S. D. Ellis, Z. Kunszt, and D. E. Soper, Phys. Rev. Lett. **62**, 726 (1989); S. Catani, Yu I. Dokshitzer, M. Seymour, and B. R. Webber, Report No. CERN-TH-6775/93.
[72] S. Kretzer, H. L. Lai, F. Olness, and W. K. Tung, Phys. Rev. D **69**, 114005 (2004); D. Stump, J. Huston, J. Pumplin, W. K. Tung, H. L. Lai, S. Kuhlmann, and J. F. Owens, J. High Energy Phys. 10 (2003) 046.
[73] M. Hirai, S. Kumano, and N. Saito, Phys. Rev. D **74**, 014015 (2006).
[74] S. S. Adler *et al.*, Phys. Rev. Lett. **93**, 202002 (2004).